

Polarization control of an X-ray free-electron laser with a diamond phase retarder

Motohiro Suzuki,^{a,b*} Yuichi Inubushi,^b Makina Yabashi^b and Tetsuya Ishikawa^b

Received 29 November 2013

Accepted 2 March 2014

^aJASRI/SPring-8, 1-1-1 Kouto, Sayo, Hyogo 679-5198, Japan, and ^bRIKEN SPring-8 Center, 1-1-1 Kouto, Sayo, Hyogo 679-5148, Japan. *E-mail: m-suzuki@spring8.or.jp

A diamond phase retarder was applied to control the polarization states of a hard X-ray free-electron laser (XFEL) in the photon energy range 5–20 keV. The horizontal polarization of the XFEL beam generated from the planar undulators of the SPring-8 Angstrom Compact Free-Electron Laser (SACLA) was converted into vertical or circular polarization of either helicity by adjusting the angular offset of the diamond crystal from the exact Bragg condition. Using a 1.5 mm-thick crystal, a high degree of circular polarization, 97%, was obtained for 11.56 keV monochromatic X-rays, whereas the degree of vertical polarization was 67%, both of which agreed with the estimations including the energy bandwidth of the Si 111 beamline monochromator.

© 2014 International Union of Crystallography

Keywords: X-ray polarization optics; X-ray free-electron lasers; circular polarization.

1. Introduction

X-ray free-electron lasers (XFELs) (Ackermann *et al.*, 2007; Emma *et al.*, 2010; Ishikawa *et al.*, 2012; Allaria *et al.*, 2012) produce brilliant transversely coherent (Vartanyants *et al.*, 2011) and ultrashort X-ray pulses (Inubushi *et al.*, 2012). The X-ray polarization property is another useful feature of an XFEL, though it has not been fully exploited. In conventional synchrotron light sources, anisotropic and magnetic properties in matter have been widely investigated using X-rays with various polarization states. Full utilization of the XFEL polarization property should expand the capability of this powerful light source. For example, control and switching of the linear polarization direction allows us to access the ultrafast directional anisotropy of matter, such as the asymmetry of chemical bonding and ordering of the electronic states. Switching between horizontal and vertical polarization would also be useful in some experiments in which the sample and/or whole set-up cannot be rotated with respect to the linear polarization, such as structural dynamics involving a liquid surface or interface, as well as ultrafast diffractometry and X-ray-emission spectroscopy using complex set-ups. Circularly polarized XFEL light can reveal the ultrafast dynamics in magnetisms (Boeglin *et al.*, 2010; Pfau *et al.*, 2012), multiferroics and chiralities in pico- to femtosecond time scales, directly probing the elemental processes involving the excitation and relaxation of electron spins and orbitals. Ultrafast magnetic imaging in a single-shot scheme would be workable with circularly polarized coherent XFEL radiation (Wang *et al.*, 2012).

However, all free-electron lasers currently operating in the hard and soft X-ray regions generate only a linearly polarized beam of a fixed direction in the horizontal plane, and variable

X-ray polarization is not available. A technique for controlling the XFEL polarization states is highly sought, and, in particular, the generation and utilization of circularly polarized XFEL radiation are strongly demanded.

For a generation of XFEL beams with variable polarization states, schemes based on specially designed undulator devices have been proposed. The so-called ‘afterburner’ technique (Schneidmiller & Yurkov, 2010; Allaria *et al.*, 2011; Geloni *et al.*, 2011) uses helical or crossed-planar undulators at the last stage of the self-amplified spontaneous-emission (SASE) radiator. In the vacuum ultraviolet region, FERMI@Elettra has begun operation delivering circularly polarized FEL pulses at wavelengths of 20–32 nm using APPLE-II type undulators (Allaria *et al.*, 2012). With an APPLE-type undulator to generate circular polarization (Sasaki, 1994), the photon helicities are basically fixed but variable by a slow mechanical movement of the undulator magnet blocks. Another scheme using crossed-planar undulators with a phase shifter (Kim, 2000; Schneidmiller & Yurkov, 2010) has been proposed for arbitrary polarization control. Polarization states can be switched by AC-activation of the phase shifter. For faster polarization switching, an electromagnetic helical undulator implemented into the afterburner scheme might be a possible option. These methods are particularly suitable for the soft X-ray region where practical X-ray polarization optics are unavailable. However, these polarization control techniques based on special undulators are currently under development and further technical challenges may need to be overcome for practical operation.

In the hard X-ray region, another convenient technique that utilizes crystal optics has been established (Hirano *et al.*, 1991; Giles *et al.*, 1994; Lang & Srajer, 1995) for conventional synchrotron radiation. A diamond crystal in the Bragg/Laue

transmission geometry can work as a phase retarder to switch the polarization states of hard X-rays with high efficiency. This type of diamond X-ray phase retarder (XPR) offers several benefits including (i) a high degree of polarization with high throughput, (ii) wide tunability in X-ray wavelengths (Hirano *et al.*, 1992*b*) and (iii) fast polarization switching (Hirano *et al.*, 1992*a*; Suzuki *et al.*, 1998, 2003). Thus, diamond XPRs have been widely used at storage-ring-based synchrotron light sources.

In this study, we applied crystal optics to control the polarization states of XFEL radiation. At SPring-8 Angstrom Compact Free Electron Laser (SACLA), we used the set-up of a diamond XPR similar to that commonly adopted in many synchrotron beamlines to investigate the performance of the XPR for an XFEL beam. The horizontal polarization of XFEL radiation generated from planar undulators of SACLA was successfully converted to vertical or circular polarization of either helicity. We describe the performance of the XPR and the polarization characteristics obtained for hard X-rays at 11.56 keV.

2. Polarization control using a crystal phase retarder

2.1. Principle

In the general set-up of a diffractive XPR in the transmission geometry (Hirano *et al.*, 1991; Giles *et al.*, 1994; Lang & Srajer, 1995), a crystal is used with a diffraction plane rotated by 45° from the horizontal plane. An incident electromagnetic wave of horizontal polarization can be decomposed into the σ - and π -polarization components with respect to the diffraction plane, which have the same amplitudes and are oscillating in phase. Phase retardation between these two components occurs near the Bragg condition, and the polarization states can be converted by changing the retardation. According to the dynamical theory of diffraction, the phase retardation generated by an XPR of thickness t at an angular offset of $\Delta\theta = \theta - \theta_B$ is given by

$$\delta = -\frac{\pi}{2} \left[\frac{r_c^2 \text{Re}(F_h F_{\bar{h}}) \lambda^3 \sin 2\theta_B}{\pi^2 V^2 \Delta\theta} \right] \frac{t}{\cos \theta} = -\frac{\pi}{2} \frac{At}{\Delta\theta}, \quad (1)$$

where r_c is the classical electron radius, F_h and $F_{\bar{h}}$ are the structure factor of the hkl and $\bar{h}\bar{k}\bar{l}$ reflections, respectively, V is the unit-cell volume, λ is the X-ray wavelength, θ_B is the Bragg angle, and $A = r_c^2 \text{Re}(F_h F_{\bar{h}}) \lambda^3 \sin 2\theta_B / \pi^2 V^2 \cos \theta$. The incoming horizontal polarization can be converted into circular polarization at the crystal angle $\Delta\theta = \pm At$ at which the XPR generates $\delta = \mp\pi/2$ retardation. Vertical linear polarization can be obtained at $\Delta\theta = \pm At/2$ at which $\delta = \mp\pi$ retardation is generated.

By assuming that a perfect horizontally polarized beam is incoming to the XPR, the degree of circular polarization of the transmitted beam is defined by

$$P_C = \frac{I_R - I_L}{I_R + I_L} = \sin \delta, \quad (2)$$

Table 1

Parameters of the diamond crystals used for X-ray phase retarders.

| Thickness | Dimensions | Orientation | Geometry | X-ray energy |
|-----------|-------------|-------------|--------------------|--------------|
| 0.1 mm | 5 mm × 5 mm | (1 1 0) | 111 symmetric Laue | 5–8 keV |
| 0.5 mm | 8 mm × 4 mm | (1 1 1) | 220 symmetric Laue | 8–12 keV |
| 1.5 mm | 8 mm × 8 mm | (1 0 0) | 220 symmetric Laue | 12–16 keV |

where I_R and I_L are the intensities of the circular polarization components for right- and left-helicities, respectively. The degree of linear polarization of the transmitted beam is written as

$$P_L = \frac{I_H - I_V}{I_H + I_V} = \cos \delta, \quad (3)$$

where I_H and I_V denote the intensities of the horizontal and vertical linear polarization components, respectively. Note that $P_L = +1$ for perfect horizontal linear polarization, and $P_L = -1$ for perfect vertical linear polarization.

For an incident X-ray beam with a finite energy bandwidth and/or angular divergence, the effective angular offset will have some dispersion, and the resulting phase retardation δ will not be the ideal value given by equation (1). This may cause degradation of the XPR-converted polarization states, and the degree of circular polarization P_C and linear polarization P_L may be reduced. For a constant energy bandwidth and angular divergence, the degradation effect should be greater for a thinner crystal and at a higher X-ray energy because the slope of the phase retardation,

$$\left. \frac{d(\delta)}{d(\Delta\theta)} \right|_{\Delta\theta_c} = \pi/2At,$$

increases for both small t and λ with respect to the crystal angle.

2.2. Diamond crystals and expected performances

We used synthetic diamond crystals of IIa grade, fabricated under high-pressure and high-temperature conditions (Sumiya & Tamasaku, 2012). All crystals were provided by Sumitomo Electric Industries Ltd. Table 1 summarizes the parameters of the diamond XPR crystals. We designed three crystals of different thicknesses, 0.1, 0.5 and 1.5 mm, to cover a wide X-ray energy range between 5 and 20 keV. By selecting an appropriate crystal, we may control the X-ray polarization states for the whole X-ray energy range currently available at SACLA.

Fig. 1 shows calculated performances of the diamond XPRs. The degree of circular polarization, P_C , the transmittance, $T = \exp(-\mu t / \cos \theta)$, with the linear absorption coefficient of diamond, μ , and the figure of merit¹, $M = P_C T^{1/2}$, are plotted for the three crystals as a function of the X-ray energy. The thick curves represent the results assuming an energy bandwidth of $\Delta E/E = 1.1 \times 10^{-4}$, currently available in the

¹ The figure-of-merit in this formula indicates the signal-to-noise ratio of an X-ray magnetic circular dichroism measurement because the dichroic signal is proportional to P_C and the statistical accuracy increases with the square root of the number of photons, namely $T^{1/2}$.

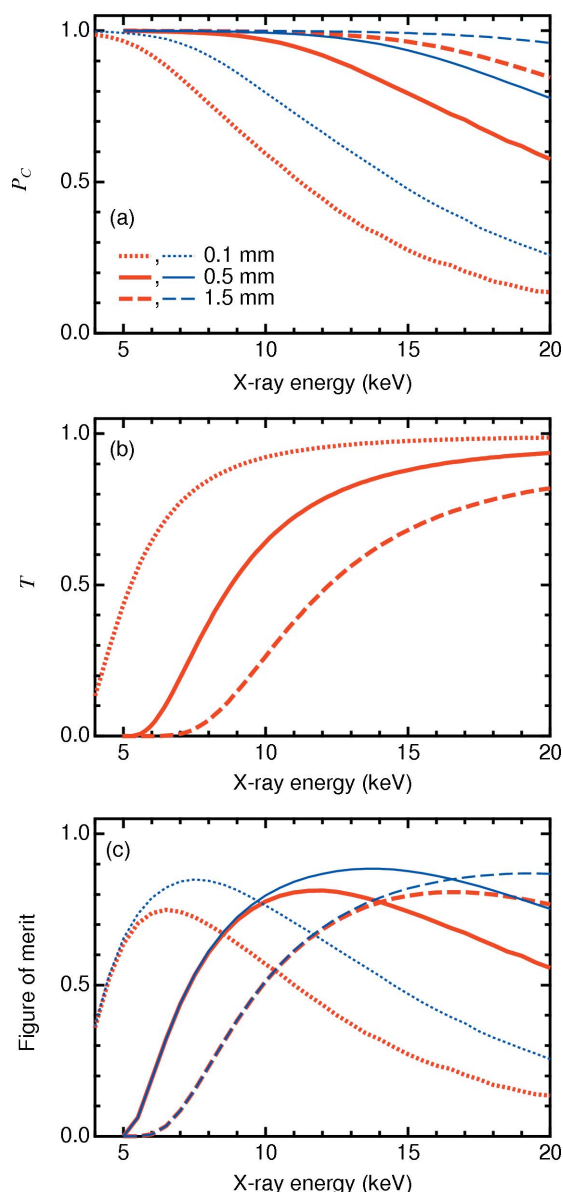


Figure 1 Expected performances of diamond phase retarders with crystal thicknesses of 0.1 (dotted), 0.5 (solid) and 1.5 mm (long dashed lines) plotted as a function of the X-ray energy: (a) degree of circular polarization, P_C , (b) transmittance, T , and (c) figure of merit, $M = P_C T^{1/2}$. Thick and thin lines represent the calculation results assuming an X-ray energy bandwidth of $\Delta E/E = 1.1 \times 10^{-4}$ and 0.5×10^{-4} , respectively.

monochromatic mode at SACLA. The thinnest 0.1 mm crystal used in the 111 Laue geometry shows a reasonable degree of circular polarization and high transmittance in the low-energy region of 5–8 keV. In the 8–14 keV X-ray energy, the 0.5 mm-thick crystal used in the 220 Laue geometry works properly with a high P_C and moderate T . The thickest 1.5 mm crystal is best suited for high-energy X-rays up to 20 keV. We obtained figure-of-merit values of $M > 0.6$ for the whole energy region (5–20 keV) when the appropriate crystal was used as specified above.

To study the capabilities of XPR for highly monochromatic self-seeded XFEL radiation (Amann *et al.*, 2012), available in the near future, thin curves in Figs. 1(a) and 1(c) show P_C and M , respectively, for the same crystals when used for an X-ray beam with a narrower bandwidth of $\Delta E/E = 0.5 \times 10^{-4}$. The degrees of circular polarization P_C are shown to increase by up to 0.2 at higher X-ray energies when the bandwidth is reduced to approximately half. Correspondingly, the figure-of-merits M would increase by ~ 0.1 and the maxima move to the higher energy side by ~ 2 keV. The transmittance T does not depend on the bandwidth. The set of three diamond crystals can provide a high degree of circular polarization with a good polarization-conversion efficiency for the SASE radiation currently available. The performances of the XPR could be further improved with the use of forthcoming seeded XFEL radiation.

3. Experiment

3.1. Instrumentation

The diamond XPR has been installed on the BL3 beamline at SACLA, which delivers linearly polarized XFEL radiation between 4.5 and 19.5 keV (Tono *et al.*, 2013). Fig. 2 shows the beamline layout, including the front-end section and the components in the optics hutch. The XPR requires a monochromatic X-ray beam, and therefore it should be used in the monochromatic mode of BL3 (Tono *et al.*, 2013). A vacuum chamber dedicated to the XPR was installed near the end of the optics hutch, between the gas monitor (GM) and the second beam monitor (BM2). We designed our XPR system to be one of the optical components of the beamline, installed permanently, and routinely used for relevant user experiments.

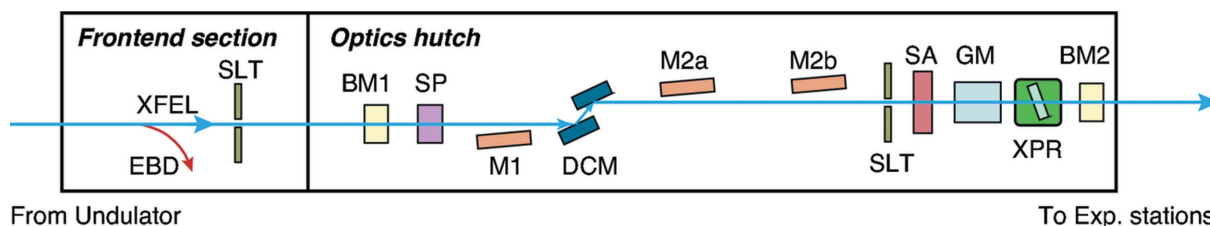


Figure 2 Layout of the BL3 beamline at SACLA, presented with the major optical components in the front-end section and optics hutch. The components include the electron beam dump (EBD), aperture slits (SLT), beam monitors (BM1 and BM2), spectrum monitor (SP), mirrors (M1, M2a, M2b), Si double-crystal monochromator (DCM), solid attenuator (SA), gas monitor (GM) and X-ray phase retarder (XPR).

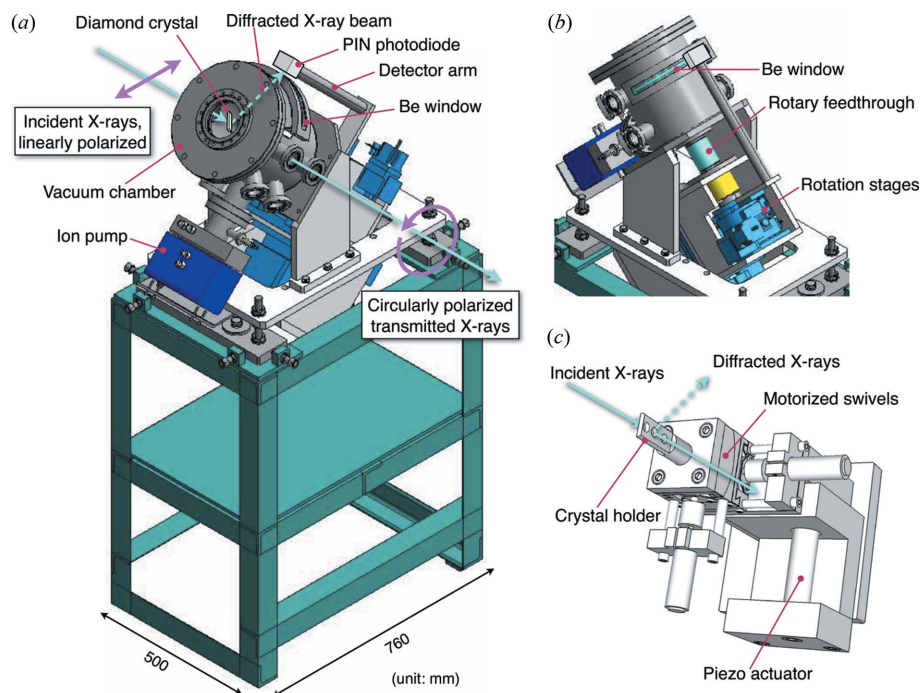


Figure 3
 (a) Vacuum chamber for the X-ray phase retarder installed in the optics hutch at BL3, SACLA. (b) Back view: the Be window used for taking the diffracted X-ray beam out of the chamber, the coaxial rotation stages, and the rotary feedthrough. (c) Piezo-driven crystal stage.

Fig. 3(a) shows an external view of the vacuum chamber. The main cylinder body axes and the rotation axis of the diamond crystal are coaxial, and they are tilted by 45° from the horizontal plane. In Fig. 3(b) a Be slit window is placed on the cylinder body side for taking the diffracted X-ray beam out of the chamber. The diamond XPR crystal is located in the centre of the chamber. A magnetic fluid-coupling feedthrough transmits the ω rotation to the crystal inside the chamber, while maintaining a vacuum of better than $\leq 5 \times 10^{-5}$ Pa. The crystal translations in the plane perpendicular to the X-rays are attained by X–Y stepping-motor stages outside the vacuum. Together with the motorized stages, a piezo-driven stage was adopted for quick fine-tuning of the crystal angle (Hirano *et al.*, 1992a; Suzuki *et al.*, 1998). Fig. 3(c) shows the piezo stage, which is vacuum compatible and placed onto an ω

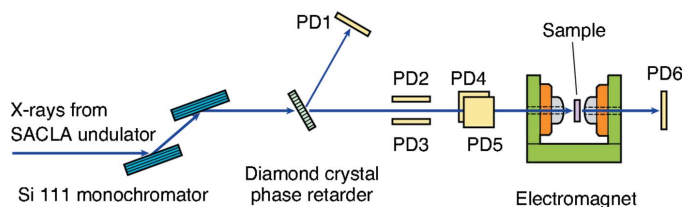


Figure 4
 Experimental set-up for polarization measurement at the SACLA BL3 beamline. Here, PD1–PD6 represent silicon PIN photodiodes. PD1 was used to monitor the X-ray intensity diffracted from the diamond phase retarder crystal. PD2, PD3, PD4 and PD5 were used to determine the degree of linear polarization by monitoring the intensities of the Thomson scattering by air in the vertical and horizontal directions. PD6 measured the transmitted intensity through the ferromagnetic sample.

rotation table inside the chamber. This set-up enables fast angular oscillation of the XPR crystal at 100 Hz for sinusoidal motion and at 40 Hz for rectangular motion. Polarization switching at these frequencies is feasible. Our XPR system may allow shot-to-shot polarization switching synchronizing with the XFEL pulses at 60 Hz, the maximum repetition frequency of SACLA.

3.2. Polarization measurements

The measurement of X-ray polarization states was carried out at experimental hutch 2 at BL3, using the experimental set-up shown in Fig. 4. SACLA was operated at a repetition rate of 10 Hz. The XFEL radiation from the BL3 undulator was monochromated using a Si 111 double-crystal monochromator, and the 11.56 keV horizontally polarized X-ray beam was incident on the XPR. We chose the 1.5 mm-thick crystal to attempt a consistent demonstration of generating vertical and circular polarization with a high degree

using the same crystal although the figure-of-merit M for circular polarization is the greatest for the thinner 0.5 mm crystal at this X-ray energy (see Fig. 1c). The crystal plane orientation was (001), and the symmetric 220 Laue geometry was used. The rocking curve of the diamond 220 reflection was symmetric and was 11 arcsec full width at half-maximum (FWHM).

4. Results and discussion

4.1. Vertical polarization

The degree of linear polarization was measured using the Thomson scattering intensities from air. Si photodiodes (PDs), PD2 and PD3, were placed above and below the X-ray beam path to monitor the air-scattered X-rays in the vertical plane, which corresponds to the intensity of the horizontal polarization component. PD4 and PD5 were placed to the right and left of the X-ray beam to monitor the intensities scattered in the horizontal plane, which corresponds to the intensity of the vertical polarization component.

Fig. 5(a) shows the X-ray intensities scattered in the vertical plane I_x (closed circles) and in the horizontal plane I_y (open squares), as a function of the XPR crystal angular offset, $\Delta\theta$, measured from the exact Bragg condition. Here, $I_x = (I_2 + I_3)/I_6$ and $I_y = (I_4 + I_5)/I_6$ were the sum of the photodiode outputs that monitored the scattering intensities in each direction (I_2 and I_3 for vertical, and I_4 and I_5 for horizontal). This was normalized by the total X-ray intensity, I_6 , which was measured with PD6. Note that no samples were placed before

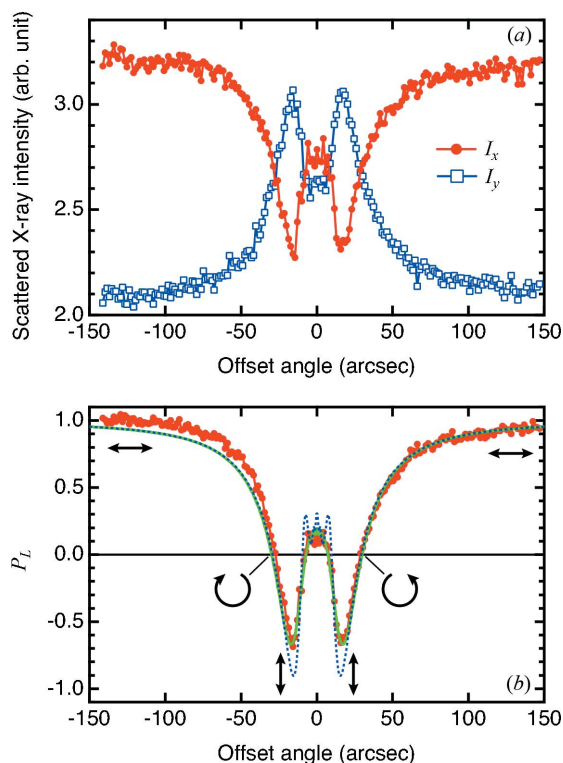


Figure 5
 (a) Output of the air-scattering polarization monitors as a function of the angular offset of an X-ray phase retarder crystal. Here, I_x (I_y) represents the X-ray intensities scattered in the vertical (horizontal) direction, corresponding to the intensity of the horizontal (vertical) polarization component. (b) The measured linear polarization rate P_L (dots) compared with the calculated results using bandwidths of $\Delta E/E = 1.1 \times 10^{-4}$ (solid line) and 0.5×10^{-4} (dotted line). Arrows represent the X-ray polarization states obtained at different offset angles.

PD6 in the linear polarization measurement. For each data point acquired, 20 XFEL pulses were averaged.

The plots of I_x and I_y in Fig. 5(a) demonstrate the X-ray polarization state varying with the change in offset angle. The horizontal polarization component, I_x , is of high value at angles far from the Bragg angle ($|\Delta\theta| > 100$ arcsec), gradually decreasing as the angle of XPR reaches the Bragg condition. The minimum I_x values occur at $\Delta\theta = \pm 16$ arcsec. The vertical polarization component I_y has the opposite behaviour.

The degree of linear polarization, P_L , was determined using the measured signals I_x and I_y and with the equation

$$P_L = \frac{1}{Q} \frac{I_x - I_y}{I_x + I_y} \quad (4)$$

where Q is the efficiency of our polarization monitor based on the air scattering of X-rays. The efficiency was estimated to be $Q = 0.213 \pm 0.001$ by a measurement for the horizontally polarized beam, which originally radiated from SACLA with no XPR inserted in the X-ray beam path. Fig. 5(b) represents the measured P_L as a function of the XPR crystal angular offset. At both sides of the Bragg condition at $\Delta\theta = \pm 16$ arcsec, the vertical linear polarization with $P_L = -0.67 \pm 0.02$ was obtained. At $\Delta\theta = -27$ and 29 arcsec, P_L crosses zero, where the XPR generates $\pm\pi/2$ phase retardation, and we

obtain circular polarization with right- and left-helicity, respectively.

The solid curve in Fig. 5(b) shows P_L calculated using equation (1) and the relation of $P_L = \cos\delta$. In this calculation the effect of the monochromator bandwidth of $\Delta E/E = 1.1 \times 10^{-4}$ was assumed. The measured variation of P_L with the XPR angle was in good agreement with dynamical theory calculation. The measurement and calculation perfectly agreed for the positive offset angle, while a small discrepancy has been observed in the negative offset angle, where $\Delta\theta < -50$ arcsec. The asymmetry in the measured profile is probably due to a simultaneous reflection that occurred accidentally near the 220 reflection used for polarization control. In fact, a small glitch was found around $\Delta\theta = -280$ arcsec, and the tail of the glitch could affect the polarization states of the transmitted beam. The glitch can be removed by changing the azimuth of the XPR crystal by $\sim 1.0^\circ$, and the resulting P_L profiles coincide with theory.

4.2. Circular polarization

For circular polarization measurements, we used the X-ray magnetic circular dichroism (XMCD) effect of a ferromagnetic sample. Fine powders of CoPt₃ ordered alloy (Maruyama *et al.*, 1995) were spread onto Scotch tape for X-ray absorption measurements in the transmission mode. The sample magnetization was saturated in the direction parallel or antiparallel to the X-ray wavevector using an electromagnet. The X-ray energy was tuned to 11.562 keV at the Pt L_3 -edge at which the maximum XMCD effect was expected (Maruyama *et al.*, 1995).

Fig. 6 shows the measured variation of the magnetic asymmetry ratio

$$R = \frac{I^+/I_0^+ - I^-/I_0^-}{I^+/I_0^+ + I^-/I_0^-}, \quad (5)$$

as a function of the offset angle of XPR, where I^+ (I^-) is the intensity, measured by PD6, and transmitted through the CoPt₃ sample for a magnetic field of 1.2 T applied in the direction antiparallel (parallel) to the X-ray propagation

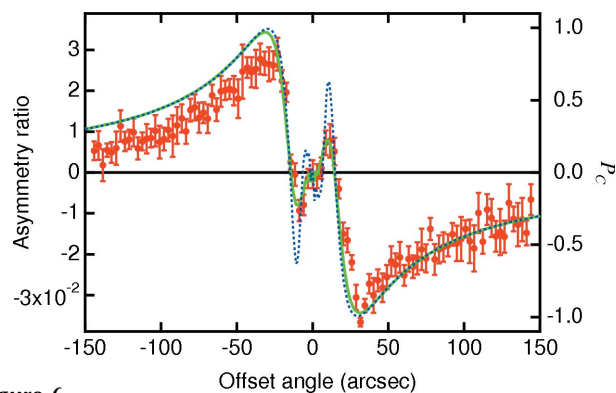


Figure 6
 Magnetic asymmetry ratio (dots) recorded for the CoPt₃ alloy at the Pt L_3 -edge as a function of the offset angle of the X-ray phase retarder crystal. The asymmetry ratio is compared with the calculated circular polarization rate, assuming bandwidths of $\Delta E/E = 1.1 \times 10^{-4}$ (solid line) and 0.5×10^{-4} (dotted line).

direction. Here, I_0^+ (I_0^-) is the intensity of the incident X-ray beam, which is the sum of the output of PD2–PD5. The measured asymmetry ratio R corresponds to the XMCD effect and should be proportional to the degree of circular polarization P_C . At each measurement point, we averaged 450 XFEL pulses for both magnetization directions. The acquisition time was 90 s per point. It should be noted that the magnetic signal (magnitude of R) was only about 3%. For comparison, a calculated P_C value is also shown in Fig. 6. We assumed the energy bandwidth was the same as that used for calculation of P_L (Fig. 5*b*). The scale factor between the asymmetry ratio R and P_C was determined by a separate XMCD measurement of the same sample at the synchrotron beamline BL39XU of SPring-8.

The measured magnetic asymmetry R is in good agreement with the calculated variation of P_C for positive offset angles. We obtained nearly perfect circular polarization of $P_C = -0.97 \pm 0.06$ at $\Delta\theta = 31$ arcsec. However, for negative offset angles, the highest value is only $P_C = 0.82 \pm 0.06$, which is lower than the values expected from the calculation. The purity of circular polarization was probably degraded by the glitch at $\Delta\theta = -280$ arcsec, as discussed above. The averaged intensity of the circularly polarized XFEL beam was estimated to be 0.55 μJ per pulse using the output of the BM2 monitor and the transmittance of the XPR. The diamond XPR successfully generated circular polarization from the original linear polarization of SACLA at 11.562 keV. The measured polarization state and the optimum offset angle were in good agreement with the dynamical theory calculation. The XMCD effects were observed at the Pt L_3 -edge in the CoPt₃ magnetic alloy using circularly polarized XFEL radiation.

The obtained degree of circular polarization, $|P_C| = 0.97$, is comparable with the values available using a similar set-up at a synchrotron beamline (Suzuki *et al.*, 2003), being sufficiently high for most state-of-the-art XMCD experiments. Possible loss in the measured dichroic signals will be only 3% with respect to the full signal intensity expected for a perfect circular polarization since an XMCD signal is proportional to P_C . Meanwhile, the degree of vertical polarization was $P_L = -0.67$. A higher degree of vertical polarization may be necessary for some experiments detecting tiny polarization-dependent signals. Generally, as stated in §2.1, the possible sources of the depolarization effect are the angular divergence and energy spread of the X-ray beam. For an XFEL beam in monochromatic mode at BL3, SACLA, the typical angular divergence is 2.4 μrad (0.5 arcsec) (Tono *et al.*, 2013), which is negligibly small. The energy bandwidth is $\Delta E/E \simeq 1 \times 10^{-4}$, which corresponds to an effective angular dispersion to the XPR of 10 arcsec for the present geometry at 11.56 keV. The energy spread should dominantly contribute to the depolarization and limit the degree of vertical polarization. In Fig. 5(*b*), the dotted line represents the variation of P_L calculated using a narrower bandwidth of $\Delta E/E \simeq 0.5 \times 10^{-4}$. A higher degree of vertical polarization of $P_L = -0.91$ may be obtained with the same set-up when used for an X-ray beam with a smaller energy spread, which is comparable with that available with seeded XFEL (Amann *et al.*, 2012). Fig. 6

compares the dependence of P_C on the energy bandwidth; P_C does not increase much for the smaller energy spread since the original value has already been close to unity. It should be noted that a double-phase-plate set-up has been proposed to compensate the effect of the energy spread (Scagnoli *et al.*, 2009; Okitsu *et al.*, 2002). This set-up may be implemented to achieve a high degree of vertical polarization at a SASE beamline.

5. Summary and perspective

A diamond X-ray phase retarder has been applied to control the polarization states of XFEL radiation from SACLA. The crystal successfully converted a horizontally polarized 11.56 keV monochromatic XFEL beam into a vertically or circularly polarized beam of either helicity. The measured polarization state and the optimum offset angle were in good agreement with dynamical theory calculations. The XMCD signals at the Pt L_3 -edge of the CoPt₃ ferromagnetic alloy were recorded using circularly polarized XFEL beams and were used to determine the degree of circular polarization produced. In the measurement, the asymmetry ratio R has been determined by reversing the magnetic field. Our next step is to record XMCD signals by reversing the XFEL photon helicities using the XPR. Shot-to-shot polarization switching of XFEL pulses is also under development.

Various polarization-dependent studies, including time-resolved spectroscopy/diffraction, resonant X-ray scattering and coherent diffraction imaging, can be realised with the full polarization tuning capabilities of XFELs. Moreover, X-ray polarization control using XPR can be combined with a micro-focused XFEL beam (Yumoto *et al.*, 2012). At the BL39XU synchrotron beamline at SPring-8, a circularly polarized X-ray beam can be focused down to 100 nm through a combination of the diamond XPR and Kirkpatrick–Baez (KB) mirrors. We did not observe any XPR influence on the focused beam size (Suzuki *et al.*, 2013). In our preliminary study at SACLA, a focused beam spot of 1.3 $\mu\text{m} \times 1.3 \mu\text{m}$ was obtained using KB mirrors in conjunction with the XPR.

As discussed in §2.2 and §4.2, the degrees of polarization are expected to increase for an X-ray beam with a narrower bandwidth, which could be available from self-seeded XFELs. An additional merit from seeded XFELs would be a significant increase in the pulse intensity of circularly/vertically polarized beams. The XPR works only for a highly monochromatic X-ray beam with an energy bandwidth of the order of $\Delta E/E \simeq 10^{-4}$. For SASE radiation with a moderate spectrum bandwidth of $\Delta E/E \simeq 4 \times 10^{-3}$ from SACLA, a crystal monochromator is indispensable before the XPR, inevitably losing most intensity of the source spectrum. Meanwhile, highly monochromatic seeded XFEL radiation can be directly used for a diffractive XPR without a crystal monochromator, and the polarization conversion efficiency will be dramatically increased by a factor of several tens.

The authors would like to thank Hiroshi Maruyama for supplying the CoPt₃ sample. Special thanks to the SACLA

Engineering Team for their support in designing the XPR system and technical assistance during the experiment. A part of the XFEL experiment was performed at BL3 of SACLA with the approval of the Japan Synchrotron Radiation Research Institute (JASRI) (proposal No. 2013A8014). This work was supported by SACLA User's Equipment Development Proposal.

References

- Ackermann, W. *et al.* (2007). *Nat. Photon.* **1**, 336–342.
- Allaria, E., Ding, Y., Emma, P. J., Huang, Z., Nuhn, H. D., Rowen, M., Welch, J. & Wu, J. (2011). *Proceedings of FEL2011*, Shanghai, China, pp. 31–34.
- Allaria, E. *et al.* (2012). *Nat. Photon.* **6**, 699–704.
- Amann, J. *et al.* (2012). *Nat. Photon.* **6**, 693–698.
- Boeglin, C., Beaupaire, E., Halté, V., López-Flores, V., Stamm, C., Pontius, N., Dürr, H. A. & Bigot, J. Y. (2010). *Nature (London)*, **465**, 458–461.
- Emma, P. *et al.* (2010). *Nat. Photon.* **4**, 641–647.
- Geloni, G., Kocharyan, V. & Saldin, E. (2011). *Proceedings of FEL2011*, Shanghai, China, pp. 69–72.
- Giles, C., Malgrange, C., Goulon, J., de Bergevin, F., Vettier, C., Fontaine, A., Dartyge, E. & Pizzini, S. (1994). *Nucl. Instrum. Methods Phys. Res. A*, **349**, 622–625.
- Hirano, K., Ishikawa, T., Koreeda, S., Fuchigami, K., Kanzaki, K. & Kikuta, S. (1992a). *Jpn. J. Appl. Phys.* **31**, L1209–L1211.
- Hirano, K., Izumi, K., Ishikawa, T., Annaka, S. & Kikuta, S. (1991). *Jpn. J. Appl. Phys.* **30**, L407–L410.
- Hirano, K., Kanzaki, K., Mikami, M., Miura, M., Tamasaku, K., Ishikawa, T. & Kikuta, S. (1992b). *J. Appl. Cryst.* **25**, 531–535.
- Inubushi, Y., Tono, K., Togashi, T., Sato, T., Hatsui, T., Kameshima, T., Togawa, K., Hara, T., Tanaka, T., Tanaka, H., Ishikawa, T. & Yabashi, M. (2012). *Phys. Rev. Lett.* **109**, 144801.
- Ishikawa, T. *et al.* (2012). *Nat. Photon.* **6**, 540–544.
- Kim, K.-J. (2000). *Nucl. Instrum. Methods Phys. Res. A*, **445**, 329–332.
- Lang, J. C. & Srajer, G. (1995). *Rev. Sci. Instrum.* **66**, 1540–1542.
- Maruyama, H., Matsuoka, F., Kobayashi, K. & Yamazaki, H. (1995). *J. Magn. Magn. Mater.* **140**, 43–44.
- Okitsu, K., Ueji, Y., Sato, K. & Amemiya, Y. (2002). *Acta Cryst.* **A58**, 146–154.
- Pfau, B. *et al.* (2012). *Nat. Commun.* **3**, 1100.
- Sasaki, S. (1994). *Nucl. Instrum. Methods Phys. Res. A*, **347**, 83–86.
- Scagnoli, V., Mazzoli, C., Detlefs, C., Bernard, P., Fondacaro, A., Paolasini, L., Fabrizi, F. & de Bergevin, F. (2009). *J. Synchrotron Rad.* **16**, 778–787.
- Schneidmiller, E. A. & Yurkov, M. V. (2010). *Proceedings of FEL2010*, Malmö, Sweden, pp. 123–126.
- Sumiya, H. & Tamasaku, K. (2012). *Jpn. J. Appl. Phys.* **51**, 090102.
- Suzuki, M. *et al.* (2013). *J. Phys. Conf. Ser.* **430**, 012017.
- Suzuki, M., Kawamura, N. & Ishikawa, T. (2003). *Rev. Sci. Instrum.* **74**, 19–22.
- Suzuki, M., Kawamura, N., Mizumaki, M., Urata, A., Maruyama, H., Goto, S. & Ishikawa, T. (1998). *Jpn. J. Appl. Phys.* **37**, L1488–L1490.
- Tono, K. *et al.* (2013). *New J. Phys.* **15**, 083035.
- Vartanyants, I. A. *et al.* (2011). *Phys. Rev. Lett.* **107**, 144801.
- Wang, T. *et al.* (2012). *Phys. Rev. Lett.* **108**, 267403.
- Yumoto, H. *et al.* (2012). *Nat. Photon.* **7**, 43–47.